

Abstract

A number of numerical wind flow models have been developed for simulating wind flow at relatively fine spatial resolutions (e.g., ~ 100 m); however, there are very limited observational data available for evaluating these high resolution models. This study presents high-resolution surface wind datasets collected from an isolated mountain and a steep river canyon. The wind data are presented in terms of four flow regimes: upslope, afternoon, downslope, and a synoptically-driven regime. There were notable differences in the data collected from the two terrain types. For example, wind speeds collected on the isolated mountain increased with distance upslope during upslope flow, but generally decreased with distance upslope at the river canyon site during upslope flow. Wind speed did not have a simple, consistent trend with position on the slope during the downslope regime on the isolated mountain, but generally increased with distance upslope at the river canyon site. The highest measured speeds occurred during the passage of frontal systems on the isolated mountain. Mountaintop winds were often twice as high as wind speeds measured on the surrounding plain. The highest speeds measured in the river canyon occurred during late morning hours and were from easterly downcanyon flows, presumably associated with surface pressure gradients induced by formation of a regional thermal trough to the west and high pressure to the east. Under periods of weak synoptic forcing, surface winds tended to be decoupled from large-scale flows, and under periods of strong synoptic forcing, variability in surface winds was sufficiently large due to terrain-induced mechanical effects (speed-up over ridges and decreased speeds on leeward sides of terrain obstacles) that a large-scale mean flow would not be representative of surface winds at most locations on or within the terrain feature. These findings suggest that traditional operational weather model (i.e., with numerical grid resolutions of around 4 km or larger) wind predictions are not likely to be good predictors of local near-surface winds at sub-grid scales in complex terrain. The data from this effort are archived and available at: <http://www.firemodels.org/index.php/windninja-introduction/windninja-publications>.

High resolution observations of the near-surface wind field

B. W. Butler et al.

Title Page

Abstract

Introduction

Conclusions

References

Tables

Figures



Back

Close

Full Screen / Esc

Printer-friendly Version

Interactive Discussion



1 Introduction

Predictions of terrain-driven winds are important in regions with complex topography for a number of issues, including wildland fire behavior and spread (Sharples et al., 2012; Simpson et al., 2013), transport and dispersion of pollutants (Jiménez et al., 2006; Grell et al., 2000), simulation of convection-driven processes (Banta, 1984; Langhans et al., 2013), wind turbine siting (Chrust et al., 2013; Palma et al., 2008), and climate change impacts (Daly et al., 2010). Numerous efforts have focused on improving boundary-layer flow predictions from numerical weather prediction (NWP) models by either reducing the horizontal grid size in order to resolve finer-scale topographical features and their effects on atmospheric flow (Lundquist et al., 2010; Zhong and Fast, 2003) or adding new parameterizations to account for unresolved terrain features (Jiménez and Dudhia, 2012). Because NWP simulations are computationally demanding and suffer from inherent limitations of terrain-following coordinate systems in steep terrain (Lundquist et al., 2010), a number of high resolution diagnostic wind models have also been developed to downscale wind predictions from NWP models in order to meet the needs of the aforementioned applications (e.g., Beaucage et al., 2014). There are limited observational data available, however, to evaluate and improve such high resolution models. This paper describes a research program in which wind data were collected at very high spatial resolution under a range of meteorological conditions for two different types of complex terrain features. The datasets collected during this program enhance the archive of observational data available to evaluate high resolution models. All of the data from the field program are available at: <http://www.firemodels.org/index.php/windninja-introduction/windninja-publications>.

Fine-scale (i.e., $\sim 1\text{--}100\text{m}$) variations in topography and vegetation substantially alter the near-surface flow field through mechanical effects, such as flow separation around obstacles, enhanced turbulence from increased surface roughness and speed-up over ridges, and through thermally-driven flows induced by local differential surface heating in steep terrain (Banta, 1984; Banta and Cotton, 1982; Chrust et al., 2013).

ACPD

14, 16821–16863, 2014

High resolution observations of the near-surface wind field

B. W. Butler et al.

Title Page

Abstract

Introduction

Conclusions

References

Tables

Figures



Back

Close

Full Screen / Esc

Printer-friendly Version

Interactive Discussion



High resolution observations of the near-surface wind field

B. W. Butler et al.

[Title Page](#)[Abstract](#)[Introduction](#)[Conclusions](#)[References](#)[Tables](#)[Figures](#)[Back](#)[Close](#)[Full Screen / Esc](#)[Printer-friendly Version](#)[Interactive Discussion](#)

These local scale flow effects are critical for surface wind-sensitive processes, such as wildland fire behavior, where the near-surface wind is often the driving meteorological variable for fire rate of spread and intensity (Rothermel, 1972; Sharples et al., 2012). In order to capture these terrain-induced effects, wind modeling in complex terrain requires that surface characteristics, including terrain, vegetation, and their interactions with the atmosphere, be resolved at a high spatial resolution in order to provide accurate predictions of the near-surface flow field.

Although diagnostic wind models do not typically employ sophisticated boundary layer schemes in their flow solutions, they often incorporate parameterized algorithms for specific boundary layer effects, such as thermally-driven winds (e.g., diurnal slope flows) and non-neutral atmospheric stability (Forthofer et al., 2009; Scire et al., 2000). Evaluation of such schemes has been limited by the types of terrain features and range of meteorological conditions represented in available observational datasets. For example, the evaluations performed by Forthofer et al. (2014) were limited by available surface wind data in complex terrain. The two most widely used datasets for evaluation of high resolution wind predictions were collected on topographically-simple, low elevation hills investigated for wind energy applications (Berg et al., 2011; Taylor and Teunissen, 1987). Wind energy research has focused on relatively simple terrain because winds in complicated terrain are more difficult to reliably forecast and have higher turbulence that reduces the life of the turbines. These studies of idealized field sites have produced useful data for investigating the effects of simple terrain obstructions on average atmospheric flow and identifying specific deficiencies in numerical flow solutions; however, such sites represent relatively gentle terrain compared to the wide range of regions where terrain-induced winds occur. As a result, these data do not provide sufficient test data for evaluating spatial representation of modeled flows for commonly occurring types of terrain features, such as isolated terrain obstacles with complex geometries, dissected montane environments, and steep river canyons. Other types of observational studies, such as those designed to investigate boundary layer evolution or convection-driven processes, have focused on characterizing the vertical

**High resolution
observations of the
near-surface wind
field**B. W. Butler et al.

[Title Page](#)[Abstract](#)[Introduction](#)[Conclusions](#)[References](#)[Tables](#)[Figures](#)[Back](#)[Close](#)[Full Screen / Esc](#)[Printer-friendly Version](#)[Interactive Discussion](#)

(Fig. 2). The USRP is bordered by tall mountain ranges to the northwest and south-east. There are three prominent drainages (Big Lost River, Little Lost River, and Birch Creek) that flow southeast onto the USRP to the north and northeast of BSB (Fig. 2). These mountain-valley features contribute to thermally-driven diurnal flows and formation of convergence zones on the USRP. Nighttime down-drainage flows on the USRP are from the northeast and daytime up-drainage flows are from the southwest.

Typical summertime winds on the Snake River Plain are primarily thermally driven with strong upvalley winds during the day and relatively weaker downvalley winds at night. The regional nocturnal northeasterly drainage flows usually subside by late morning, and winds begin to rotate clockwise to southwesterly flow, then speeds increase sharply by mid-to-late afternoon. The strongest southwesterly wind events in the summer are associated with the passage of frontal systems.

Additionally, this region experiences occasional passage of very strong frontal systems which bring westerly winds that become channeled into southwesterly flow up the Lower Snake River Plain (LSRP) toward BSB (e.g. Andretta, 2002). This same westerly synoptic flow passes over the mountains to the northwest of BSB and surface winds become channeled into northerly flow down the Big Lost, Little Lost, and Birch Creek drainages and onto the USRP. This northerly flow approaches BSB from the USRP, eventually converging with the southwesterly flow somewhere in the vicinity of BSB in what is referred to as the Snake River Plain Convergent Zone (SPCZ) (Andretta, 2002; Andretta and Hazen, 1998). When an SPCZ forms, its location shifts up or down the SRP depending on the strength of the low-level winds over the USRP vs. the LSRP (Andretta, 2002). SPCZ events most commonly occur during the winter and spring, but occasionally form during other time periods as well. Although formation of the SPCZ is not a frequent phenomenon during summer conditions, we did observe a few flow events that may have been associated with the SPCZ during our field campaign. Because the strong frontal systems which lead to formation of the SPCZ result in complicated near-surface flows on and around BSB, we investigate the observed flow events possibly associated with SPCZ-like conditions in detail in Sect. 5.1.2.

High resolution observations of the near-surface wind field

B. W. Butler et al.

Title Page

Abstract

Introduction

Conclusions

References

Tables

Figures



Back

Close

Full Screen / Esc

Printer-friendly Version

Interactive Discussion



northeast of the butte from 31 August to 1 September 2010 (Fig. 1; Table 1). A tower of sonic anemometers was deployed 2 km southwest of the butte from 14 July to 18 July 2010 (Fig. 1; Table 1). Three RadioSonde launches were conducted at BSB from 31 August to 2 September 2010 (Table 2).

5 An array of 27 surface sensors was deployed in three cross-river transects at SRC from 14 July to 13 September 2011 (Fig. 1). Sodars and sonic anemometers were operated from 16 July to 18 July and 29 August to 31 August 2011 (Table 1). Sodars were located in the valley bottom on the north side of the river and at the ridgetop on the north side of the river near the east end of the field site (Fig. 1). Sonic anemometers
10 were operated on north and south ridgetops near the west end of the study area and at two locations in the valley bottom on the north side of the river (Fig. 1). Two weather stations monitored air temperature, relative humidity, precipitation, solar radiation, wind speed, and wind direction; one was located on the southern ridgetop at the east end of the field site and the other was located in the valley bottom on the north side of the river (Fig. 1). Six RadioSonde launches were conducted on 18 August 2011 (Table 2).

4 Analysis methods and terminology

The data analyses in this paper focus on the surface wind measurements and terrain influences on the surface flow characteristics determined from these measurements. All data are available in public archives as described in Sect. 6.

4.1 Partitioning surface data into flow regimes

The surface wind data were partitioned into four distinct wind regimes in order to facilitate the analysis of typical diurnal flows in the absence of strong synoptic forcing and high wind events during periods of strong synoptic forcing. The four wind regimes are:

1. a downslope regime, which included downslope and downvalley flows, forced by nighttime surface cooling under weak synoptic forcing,

High resolution observations of the near-surface wind field

B. W. Butler et al.

Title Page

Abstract

Introduction

Conclusions

References

Tables

Figures



Back

Close

Full Screen / Esc

Printer-friendly Version

Interactive Discussion



2. an upslope regime, which included upslope and upvalley flows, forced by daytime surface heating under weak synoptic forcing,
3. an afternoon regime, during which local flows were influenced by larger scale flows, either through convective mixing (at BSB) or through formation of upvalley drainage winds (at SRC) under weak synoptic forcing,
4. a synoptically forced regime, during which the normal diurnal cycle was disrupted by strong larger scale flows and local flows typically correlated with gradient level winds due to mechanically-induced turbulent mixing in the boundary layer.

The first three are analogous to the wind regimes described in Banta and Cotton (1982) and are referred to collectively in this paper as the diurnal wind regime. The diurnal wind regime persisted during periods of weak synoptic forcing. The fourth regime was included here as the field sites investigated in this study frequently experienced periods of intense large-scale synoptic forcing which generated high surface wind speeds and sufficient mechanical mixing to overcome the diurnal flow regime.

The following procedure was used to partition the surface data into these flow regimes. First, periods during which the wind speed exceeded a threshold wind speed at a surface sensor chosen to be representative of the large-scale flow at each site were partitioned into regime (4). Threshold wind speeds were selected for each site based on visual inspection of the wind speed time series data for the chosen sensors. Thresholds were selected to be speeds that were just above the typical daily peak speed for the chosen sensors. In other words, the threshold speed was only exceeded when synoptic forcing disrupted the typical diurnal wind regime at a given site. Speeds below the threshold are indicative of periods of weak synoptic forcing, during which the diurnal wind regime prevails. Sensors R2 and NM1 were chosen to be the representative sensors at BSB and SRC, respectively. R2 was located on the USRP approximately 5 km southwest of the butte. NM1 was located on the north side of the SRC at 1530 m a.s.l., roughly three-quarters of the distance from the canyon bottom to the ridgetop. These sensors were chosen because they appeared to be the least

High resolution observations of the near-surface wind field

B. W. Butler et al.

[Title Page](#)[Abstract](#)[Introduction](#)[Conclusions](#)[References](#)[Tables](#)[Figures](#)[Back](#)[Close](#)[Full Screen / Esc](#)[Printer-friendly Version](#)[Interactive Discussion](#)

influenced by the terrain and most representative of the gradient level winds. Threshold velocities of 6 and 5 m s⁻¹ were chosen for BSB and SRC, respectively (Fig. 3). Speeds below these thresholds fall within the range of diurnal wind flows reported in the literature (Horst and Doran, 1986) and visual inspection of the vector maps further confirmed this choice of threshold wind speeds, as all four regimes were clearly identified by the surface flow patterns at each site.

After filtering out the synoptically driven periods, the remaining data were then partitioned into regimes (1)–(3) based on visual inspection of the hourly vector maps. Periods which exhibited clearly defined downslope flow were partitioned into regime (1). Periods which exhibited clearly defined upslope flow were partitioned into regime (2). And afternoon periods during which the upslope regime was disturbed were partitioned into regime (3). Transition periods from one regime to another were also identified based on visual inspection of the hourly vector maps.

4.2 Data averaging

Surface wind observations were averaged over a 10 min period at the top of each hour to represent an average speed valid at the top of each hour. This averaging scheme was chosen to be representative of wind speeds from NWP forecasts. Although NWP output is valid at a particular instant in time, there is some inherent averaging in these “instantaneous” predictions. The averaging associated with a given prediction depends on the time-step and grid spacing used in the NWP model, but is typically on the order of minutes. The 10 min averages are referred to in the text as “hourly” data.

Hourly vector maps were used to visualize the spatial patterns of the wind fields for classifying flow regimes. The vector maps were produced by partitioning the hourly data into one of two categories: (1) strong synoptic forcing or (2) weak synoptic forcing (i.e., diurnal winds dominate), and then averaging the hourly data (for each sensor) within each category over the entire monitoring period. The result is an hourly average wind vector at each sensor location for each flow category. For example, a vector map for 13:00 LT under weak synoptic forcing would be produced by filtering out the

High resolution observations of the near-surface wind field

B. W. Butler et al.

Title Page

Abstract

Introduction

Conclusions

References

Tables

Figures



Back

Close

Full Screen / Esc

Printer-friendly Version

Interactive Discussion



The southwest flows are referred to as “synoptically driven upvalley” flows and the northeasterly flows are referred to as “synoptically driven downvalley” flows. Synoptically driven upvalley flows were generally associated with the passage of cold fronts from the west/southwest. Evolution of the synoptically driven downvalley flows is more complex and some potential mechanisms are described below. Wind speeds during the synoptically driven upvalley flows ranged from 2.9 to 20.3 m s⁻¹, with an average of 7.1 m s⁻¹; the downvalley flow speeds ranged from 0.1 to 24.4 m s⁻¹, with an average of 6.0 m s⁻¹. The synoptically driven downvalley (northeasterly) flows occurred less frequently than the synoptically driven upvalley (southwesterly) flow events; however, 4 distinct nighttime northeasterly flow events were observed during the monitoring period.

There are at least three potential mechanisms which may have contributed to the synoptically driven downvalley events that we observed. One mechanism is related to the SPCZ described in Sect. 2.1. Mechanical channeling of the gradient level winds by the surrounding terrain to the north and strong southwesterly flows on the SRP can create an SPCZ-like convergence zone with strong upvalley winds to the south of the zone and strong downvalley winds to the north of the zone. Winds at BSB could be southwesterly or northeasterly depending on which side of the convergence zone it was on. Another possibility is that thunderstorms in the mountains to the north of BSB could have generated gust outflows onto the SRP. Observations from the NOAA mesonet suggest that during summer months it is not uncommon to see SPCZ-like events in association with the passage of fronts or thunderstorm activity in the mountains to the north. The former will often generate strong outflows through the northern valleys, and the latter will sometimes generate outflow gust fronts. A third possibility is that surface pressure gradients, in some cases, may have contributed to the northeasterly flows. Two of the observed synoptically driven down valley flow events occurred during periods where there was a strong northeast to southwest surface pressure gradient which could have facilitated the flow; however, the other two observed synoptically driven downvalley events did not occur during periods of favorable surface pressure gradients,

High resolution observations of the near-surface wind field

B. W. Butler et al.

[Title Page](#)[Abstract](#)[Introduction](#)[Conclusions](#)[References](#)[Tables](#)[Figures](#)[Back](#)[Close](#)[Full Screen / Esc](#)[Printer-friendly Version](#)[Interactive Discussion](#)

so although surface pressure may be an influence, it was not the sole cause of these strong downvalley flow events. It is possible that any of these three mechanisms may have contributed to the observed downvalley flows on BSB.

It is interesting that during periods of synoptically driven downvalley flows wind speeds were generally higher on the southwest (leeward) side of BSB than on the northeast (windward) side. Perhaps this is because the maximum in the synoptically driven downvalley flow occurred at some higher elevation and was not well-mixed with near-surface winds due to nighttime temperature stratification in the NBL. This stratified flow could have become mixed into the surface flow at the ridgetops and pulled down the southwest side of BSB. The northeasterly flow also would have been enhanced by the nighttime downslope flow on the southwest side of BSB, thus producing stronger winds on this side as compared to the northeast (windward side), where the downslope flow would be in opposition (southwesterly) to the northeasterly flow.

5.2 SRC

5.2.1 Diurnal winds: upslope, afternoon, and downslope regimes

Sunrise ranged from 05:00 to 06:30 during the monitoring period. Upslope winds formed around 09:00 and were fully established by 10:00, peaked around 12:00 and persisted until around 15:00. The upslope regime was characterized by thermally-driven upslope winds on both sides of the canyon as well as up smaller side drainage slopes (Fig. 9). The one notable exception was sensor NM2, which experienced easterly or southeasterly flow during most periods of the day (Fig. 9). We believe this sensor was perhaps in a local recirculation zone formed in the small side drainage where this sensor was located; this is discussed at the end of this section. Wind speeds in the upslope regime ranged from 0.75 to 4.0 m s⁻¹, with an average of 2.4 m s⁻¹ (Table 3).

Wind speeds tended to be highest at the upper elevation sensors around the onset of the upslope regime at 09:00 (Fig. 10). As the upslope regime developed, wind speeds peaked around 11:00 and were highest at the mid elevation sensors (Fig. 10) and this

shift from upslope to upvalley flow with a change in wind direction, but that the highest speeds were still observed at the upper elevation sensors.

Sunset ranged from 19:00 to 20:30 during the monitoring period. Upvalley flow began to weaken and transition to downslope flow between 20:00 and 21:00. The downslope regime was fully established by 22:00 and persisted until around 07:00. Peak wind speeds in the downslope regime occurred around 22:00. Wind speeds in the downslope flow regime ranged from 0.33 to 4.1 m s⁻¹, with an average of 1.2 m s⁻¹ (Table 3). Wind speeds tended to increase with upslope distance (Fig. 11), with the exception of the SE transect, likely due to the location of SE3 and SE4 as discussed above. This trend was consistent throughout the duration of the downslope regime.

Diurnal trends were further inspected for the NM transect. We chose this transect for further investigation as this transect was not located near any prominent side drainages and likely exhibited the simplest flow characteristics. Contour plots showed a strong diurnal signal for all sensors in this transect (Fig. 12), indicating that diurnal flows are a major flow feature in the SRC. Winds were from the east/southeast in the early morning and from the west/northwest in the afternoon and the highest speeds occurred at the upper elevation sensors during early morning hours. One exception was the NM2 sensor, which rarely experienced winds from the west/northwest and did not experience a morning time peak in wind speed. This sensor was located slightly off of a mid-slope ridge on a slope with a northwest aspect. We suspect that this location was possibly a zone of recirculation. The lowest sensor, NM4, also did not experience a morning peak in wind speed and rarely experienced winds from the northeast. The highest speeds occurred during periods of synoptic disturbance, which we believe had more of an effect at upper elevations in the SRC than lower ones near the river bottom. This is discussed further in the next section.

5.2.2 Synoptic disturbance of diurnal winds

We observed two types of synoptic disturbances to the diurnal wind regime in the SRC (Fig. 13). One is associated with the passage of frontal systems from the west,

High resolution observations of the near-surface wind field

B. W. Butler et al.

Title Page

Abstract

Introduction

Conclusions

References

Tables

Figures



Back

Close

Full Screen / Esc

Printer-friendly Version

Interactive Discussion



High resolution observations of the near-surface wind field

B. W. Butler et al.

Title Page

Abstract

Introduction

Conclusions

References

Tables

Figures

◀

▶

◀

▶

Back

Close

Full Screen / Esc

Printer-friendly Version

Interactive Discussion



which brings strong westerly gradient winds. The other appears to be associated with the presence of an east-west pressure gradient that generates strong morning-time easterly flow. During the passage of frontal systems, westerly winds are channeled up the river canyon and most sensors in SRC (with the exception of those located in side drainages) experienced westerly flow. These events tended to occur during mid-afternoon hours. Wind speeds during this type of synoptic disturbance ranged from 2.1 to 5.7 m s⁻¹, with an average of 3.8 m s⁻¹.

The highest observed wind speeds in the SRC were from the east during morning hours (Figs. 12 and 13). Wind speeds during these pressure-driven downvalley events ranged from 0.84 to 9.1 m s⁻¹, with an average of 3.1 m s⁻¹. These events occurred roughly every few days and appeared to be induced by a surface pressure gradient formed when a thermal trough existed on the Columbia Plateau to the northwest of SRC and high pressure existed to the east of SRC (Fig. 14). An east-west surface pressure gradient existed on days when enhanced downvalley flow was observed. On days when the downvalley flow feature was not observed, there was no east-west surface pressure gradient. The highest wind speeds during this type of flow event were observed at the upper elevations of the SRC (Fig. 15). The east-west surface pressure gradient coupled with the typical nighttime/early morning katabatic flow in the canyon resulted in very strong downvalley winds in the SRC. This pressure-enhanced katabatic surface flow tended to be decoupled from the larger-scale gradient flow (which is typically from the west) during these pressure-driven events.

5.3 Archived data

All data are archived as downloadable SQLite databases. Access to these databases along with tools to query, process, and visualize, the data is described at <http://www.firemodels.org/index.php/windninja-introduction/windninja-publications>. Descriptions of the NOAA mesonet data and contact information regarding mesonet data access can be found at <http://www.noaa.inel.gov/capabilities/mesonet/mesonet.htm> and <http://niwc.noaa.inel.gov/> and <http://niwc.noaa.inel.gov/>.

6 Conclusions

We have presented an analysis of two high-resolution surface wind datasets, one collected from a tall isolated mountain, and the other from a steep river canyon. The wind data were analyzed and presented in terms of four flow regimes: upslope, afternoon, downslope, and a synoptically-driven regime. These datasets constitute a unique inventory of surface wind measurements at very high spatial resolution under dry summertime conditions. Public access to the archived datasets has been described.

Surface winds on and around BSB were completely decoupled from large-scale flows during upslope and downslope flow regimes, except for at the highest elevation ridgetop sensors. These ridgetop locations at BSB tended to correlate better with gradient-level winds than with the local diurnal surface flows. Surface winds in SRC were decoupled from large-scale flows except during periods of strong synoptic forcing that enhanced either upriver or downriver flows.

Wind speeds increased with distance upslope during the upslope regime at BSB, but generally decreased with distance upslope at SRC. Wind speed did not have a simple, consistent trend with position on the slope during the downslope regime at BSB, but generally increased with distance upslope at SRC. We did not observe a convective mixing regime at SRC under periods of weak synoptic forcing, only a transition from upslope to thermally-driven upriver flow.

The highest speeds measured at BSB occurred during the passage of frontal systems which generated strong southwesterly flows and during infrequent strong northwesterly flows presumably generated through SPCZ-like dynamics, thunderstorm outflows, or surface pressure gradients. Ridgetop winds were often twice as high as surface wind speeds measured on the surrounding SRP. The highest speeds measured at SRC occurred during late morning hours and were from easterly flows presumably produced by surface pressure gradients induced by formation of a thermal trough over the Columbia Plateau to the NW and high pressure to the east. The highest wind speeds

High resolution observations of the near-surface wind field

B. W. Butler et al.

Title Page

Abstract

Introduction

Conclusions

References

Tables

Figures



Back

Close

Full Screen / Esc

Printer-friendly Version

Interactive Discussion



during these pressure-driven easterly flow events were measured at the mid to high elevation sensors.

These results have important implications for modeling near-surface winds in complex terrain. The fact that surface winds at both sites tended to be decoupled from large-scale flows under periods of weak synoptic forcing suggests that traditional operational weather model winds (i.e., with numerical grid resolutions of around 4 km or larger) are not likely to be good predictors of local winds in sub-grid scale complex terrain. Under periods of strong synoptic forcing, variability in surface winds was sufficiently large due to terrain-induced mechanical effects (speed-up over ridges and decreased speeds on leeward sides of terrain obstacles), that a mean wind for a 4 km grid cell encompassing these terrain features would not be representative of actual surface winds at most locations on or within the terrain feature. The findings from this work along with the additional archived data and available mesonet data at BSB should provide guidance for future development and evaluation of high-resolution wind models and integrated parameterizations, possibly directed at the simulation of diurnal slope flows and non-neutral atmospheric stability effects.

Acknowledgements. The Department of Interior Bureau of Land Management Idaho Falls, ID field office facilitated the field campaign and Barry Sorenson provided critical advice on local conditions, access roads, and weather as well as permission to store equipment onsite during the deployment at Big Southern Butte. Thanks to N. Van Dyk, O. Martyusheva, J. Kautz, P. Robichaud, and B. Kopyscianski of the Rocky Mountain Research Station for help with the field installation and maintenance at the Salmon River site. Funding was provided by the Joint Fire Science Program, the US Forest Service, Washington State University, and the National Oceanic and Atmospheric Administration Field Research Division.

References

Andretta, T. A.: Climatology of the Snake River Plain convergence zone, National Weather Digest, 26, 37–51, 2002.

High resolution observations of the near-surface wind field

B. W. Butler et al.

Title Page

Abstract

Introduction

Conclusions

References

Tables

Figures



Back

Close

Full Screen / Esc

Printer-friendly Version

Interactive Discussion



High resolution observations of the near-surface wind field

B. W. Butler et al.

Title Page

Abstract

Introduction

Conclusions

References

Tables

Figures



Back

Close

Full Screen / Esc

Printer-friendly Version

Interactive Discussion



- Andretta, T. Z. and Hazen, D. S.: Doppler radar analysis of a Snake River Plain convergence event, *Weather Forecast.*, 13, 482–491, 1998.
- Banta, R. M.: Daytime boundary-layer evolution over mountainous terrain, Part 1: observations of the dry circulations, *Mon. Weather Rev.*, 112, 340–356, 1984.
- 5 Banta, R. M. and Cotton, R.: An analysis of the structure of local wind systems in a broad mountain basin, *J. Appl. Meteorol.*, 20, 1255–1266, 1982.
- Beaucage, P., Brower, M. C., and Tensen, J.: Evaluation of four numerical wind flow models for wind resource mapping, *Wind Energy*, 12, 197–208, doi:10.1002/we.1568, 2014.
- 10 Berg, J., Mann, J., Bechmann, A., Courtney, M. S., and Jørgensen, H. E.: The Bolund Experiment, Part I: Flow over a steep, three-dimensional hill, *Bound.-Lay. Meteorol.*, 141, 219–243, 2011.
- Chrust, M. F., Whiteman, C. D., and Hoch, S. W.: Observations of thermally driven wind jets at the exit of Weber Canyon, Utah, *J. Appl. Meteorol. Climatol.*, 52, 1187–1200, 2013.
- Daly, C., Conklin, D. R., and Unsworth, M. H.: Local atmospheric decoupling in complex topog-
 15 raphy alters climate change impacts, *Int. J. Climatol.*, 30, 1857–1864, 2010.
- Forthofer, J., Shannon, K., and Butler, B.: Simulating diurnally driven slope winds with Wind-Ninja, Eighth Symposium on Fire and Forest Meteorology, Kalispell, MT, 13–15 October, https://ams.confex.com/ams/8Fire/techprogram/paper_156275.htm (last access: 20 June 2014), 2009.
- 20 Forthofer, J. M., Butler, B.W, and Wagenbrenner, N. S.: A comparison of two approaches for simulating fine-scale winds in support of wildland fire management: Part 1 – model formulation and comparison against measurements, *Int. J. Wildland Fire*, in press, 2014.
- Geerts, B., Miao, Q., and Demko, J. C.: Pressure perturbations and upslope flow over a heated, isolated mountain, *Mon. Weather Rev.*, 136, 4272–4288, 2008.
- 25 Grell, G. A., Emeis, S., Stockwell, W. R., Schoenemeyer, T., Forkel, R., Michalakes, J., Knoche, R., and Seidl, W.: Application of a multiscale, coupled MM5/chemistry model to the complex terrain of the VOTALP valley campaign, *Atmos. Environ.*, 34, 1435–1453, 2000.
- Horst, T. W. and Doran, J. C.: Nocturnal drainage flow on simple slopes, *Bound.-Lay. Meteorol.*, 34, 263–286, 1986.
- 30 Jiménez, P. and Dudhia, J.: Improving the representation of resolved and unresolved topographic effects on surface wind in the WRF model. *J. Appl. Meteorol. Climatol.*, 51, 300–316, 2012.

High resolution observations of the near-surface wind field

B. W. Butler et al.

Title Page

Abstract

Introduction

Conclusions

References

Tables

Figures



Back

Close

Full Screen / Esc

Printer-friendly Version

Interactive Discussion



Jiménez, P., Jorba, O., Parra, R. and Baldasano, J. M.: Evaluation of MM5-EMICAT2000-CMAQ performance and sensitivity in complex terrain: high-resolution application to the northeastern Iberian peninsula, *Atmos. Environ.*, 40, 5056–5072, 2006.

Kahle, D. and Wickham, H.: ggmap: a package for spatial visualization with Google Maps and OpenStreetMap. R package version 2.3, available at: <http://CRAN.R-project.org/package=ggmap> (last access: 19 June 2014), 2013.

Langhans, W., Juerg, S., Fuhrer, O., Bieri, S., and Schär, C.: Long-term simulations of thermally driven flows and orographic convection at convection-parameterizing and cloud-resolving resolutions. *J. Appl. Meteorol. Climatol.*, 52, 1490–1510, 2013.

Lundquist, K. A., Chow, F. K., and Lundquist, J. K.: An immersed boundary method for the weather research and forecasting model, *Mon. Weather Rev.*, 138, 796–817, 2010.

McNider, R. T. and Pielke, R. A.: Diurnal boundary-layer development over sloping terrain, *J. Atmos. Sci.*, 38, 2198–2212, 1981.

Palma, J. M. L. M., Castro, F. A., Ribeiro, L. F., Rodrigues, A. H., and Pinto, A. P.: Linear and nonlinear models in wind resource assessment and wind turbine micro-siting in complex terrain, *J. Wind Eng. Ind. Aerod.*, 96, 2308–2326, 2008.

R Core Team: R: a language and environment for statistical computing, R Foundation for Statistical Computing, Vienna, Austria, available at: <http://www.R-project.org/> (last access: 19 June 2014), 2013.

Reiter, E. R. and Tang, M.: Plateau effects on diurnal circulation patterns, *Mon. Weather Rev.*, 112, 638–651, 1984.

Rothermel, R. C.: A Mathematical Model for Predicting Fire Spread in Wildland Fuels: Ogden, UT, USDA Forest Service, Research Paper INT-115, 40 pp., 1972.

Salabim, T.: Metvurst: meteorological visualization utilities using R for science and teaching, available at: <https://github.com/tim-salabim/metvurst> (last access: 19 June 2014), 2013.

Scire, J. S., Robe, F. R., Fernau, M. E., and Yamartino, R. J.: A User's Guide for the CALMET Meteorological Model, Earth Tech, Inc., Concord, MA, 2000.

Sharples, J. J., McRae, R. H. D., and Wilkes, S. R.: Wind-terrain effects on the propagation of wildfires in rugged terrain: fire channeling, *Int. J. Wildland Fire*, 21, 282–296, 2012.

Simpson, C. C., Sharles, J. J., Evans, J. P., and McCabe, M. F.: Large eddy simulation of atypical wildland fire spread on leeward slopes, *Int. J. Wildland Fire*, 22, 599–614, 2013.

Taylor, P. A. and Teunissen, H. W.: The Askervein Hill Project: overview and background data, *Bound.-Lay. Meteorol.*, 39, 15–39, 1987.

Wagenbrenner, N. S., Lamb, B. K., Forthofer, J. M., Shannon, K. S., and Butler, B. W.: Effect of model horizontal grid resolution on near-surface wind predictions in complex terrain: evaluations with high-resolution field observations from an isolated mountain and a steep river canyon, *J. Appl. Meteorol. Climatol.*, in preparation, 2014.

- 5 Zhong, S. and Fast, J.: An evaluation of MM5, RAMS, and Meso-Eta models at subkilometer resolution using VTMX field campaign data in the Salt Lake valley, *Mon. Weather Rev.*, 131, 1301–1322, 2003.

ACPD

14, 16821–16863, 2014

High resolution observations of the near-surface wind field

B. W. Butler et al.

Title Page

Abstract

Introduction

Conclusions

References

Tables

Figures



Back

Close

Full Screen / Esc

Printer-friendly Version

Interactive Discussion



High resolution observations of the near-surface wind field

B. W. Butler et al.

Title Page

Abstract

Introduction

Conclusions

References

Tables

Figures



Back

Close

Full Screen / Esc

Printer-friendly Version

Interactive Discussion



Table 1. Sonic anemometer and vertical profiling sensor details.

ID	Site*	Sensor	Model	Time Period	Averaging Period
WSU1	BSB	Sodar	Scintech	14 Jul–15 Jul 2010	30 min
		Sonic	ATI	14 Jul–18 Jul 2010	10 Hz
WSU2	BSB	Sodar	Scintech	15 Jul–19 Jul 2010	30 min
				31 Aug–1 Sep 2010	30 min
NOAA1	BSB	Sodar	Radian 600PA	14 Jul–19 Jul 2010	30 min
		Radar	Radian LAP-3000	14 Jul–19 Jul 2010	30 min
NOAA2	BSB	Sodar	ASC 4000	14 Jul–19 Jul 2010	30 min
		ST1	Weather station	Viasala, WXT	16 Aug–12 Sep 2011
ST2	SRC	Sonic	CSAT3	18 Aug–19 Aug 2011	10 Hz
		Sodar	Scintech	16 Aug–18 Aug 2011	30 min
				29 Aug–31 Aug 2011	30 min
ST3	SRC	Sonic	ATI	16 Aug–18 Aug 2011	10 Hz
		Weather station	Viasala, WXT	17 Aug–12 Sep 2011	15 min
ST4	SRC	Sonic	ATI	16 Aug 19–Aug 2011	10 Hz

* BSB = Big Southern Butte; SRC = Salmon River Canyon.

ACPD

14, 16821–16863, 2014

High resolution observations of the near-surface wind field

B. W. Butler et al.

[Title Page](#)
[Abstract](#)
[Introduction](#)
[Conclusions](#)
[References](#)
[Tables](#)
[Figures](#)
[Back](#)
[Close](#)
[Full Screen / Esc](#)
[Printer-friendly Version](#)
[Interactive Discussion](#)


Table 2. Radiosonde launches at BSB and SRC. Times are LT.

Site*	Date	Time of launch
BSB	31 Aug 2010	16:57
	1 Sep 2010	16:59
	2 Sep 2010	10:35
SRC	18 Jul 2011	11:28
		13:56
		15:50
		18:14
		20:00
		21:32

* BSB = Big Southern Butte; SRC = Salmon River Canyon.

High resolution observations of the near-surface wind field

B. W. Butler et al.

Title Page

Abstract

Introduction

Conclusions

References

Tables

Figures



Back

Close

Full Screen / Esc

Printer-friendly Version

Interactive Discussion



Table 3. Measured wind speeds (m s^{-1}) during upslope, downslope, and afternoon regimes at Big Southern Butte (BSB) and Salmon River Canyon (SRC). Decoupled ridgetop locations (sensors R26, R35, TSW7, and R15) were omitted from BSB averages; speeds in parentheses include ridgetop sensors.

Site	Wind Speed	Upslope (11:00 LT)	Afternoon (16:00 LT)	Downslope (00:00 LT)
BSB	Min (m s^{-1})	1.8	2.3	1.3
	Max (m s^{-1})	4.5 (7.3)	8.1	7.5 (12.0)
	Mean (m s^{-1})	3.0 (3.1)	4.1	3.4 (3.7)
SRC	Min (m s^{-1})	0.75	0.92	0.33
	Max (m s^{-1})	4.0	4.2	4.1
	Mean (m s^{-1})	2.4	2.5	1.2

High resolution observations of the near-surface wind field

B. W. Butler et al.

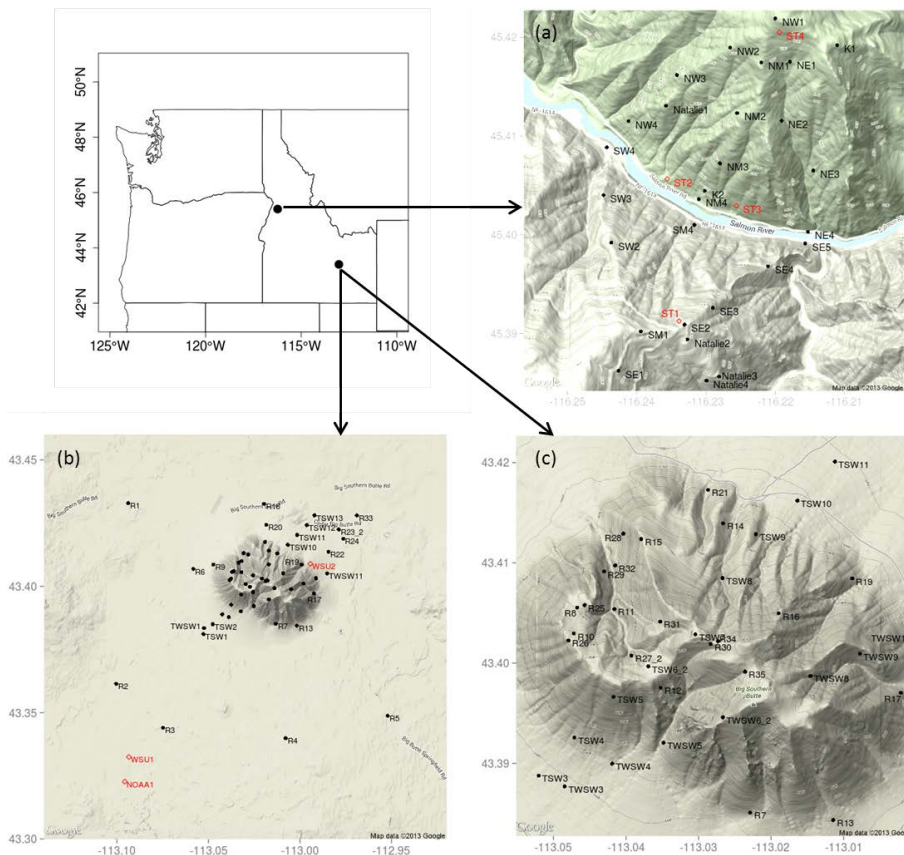


Figure 1. Site overview and sensor layouts at the Salmon River Canyon (a) and Big Southern Butte (b, c). Black circles indicate surface sensors. Red diamonds indicate sonic anemometers and vertical profiling sensors.

Title Page

Abstract Introduction

Conclusions References

Tables Figures

◀ ▶

◀ ▶

Back Close

Full Screen / Esc

Printer-friendly Version

Interactive Discussion

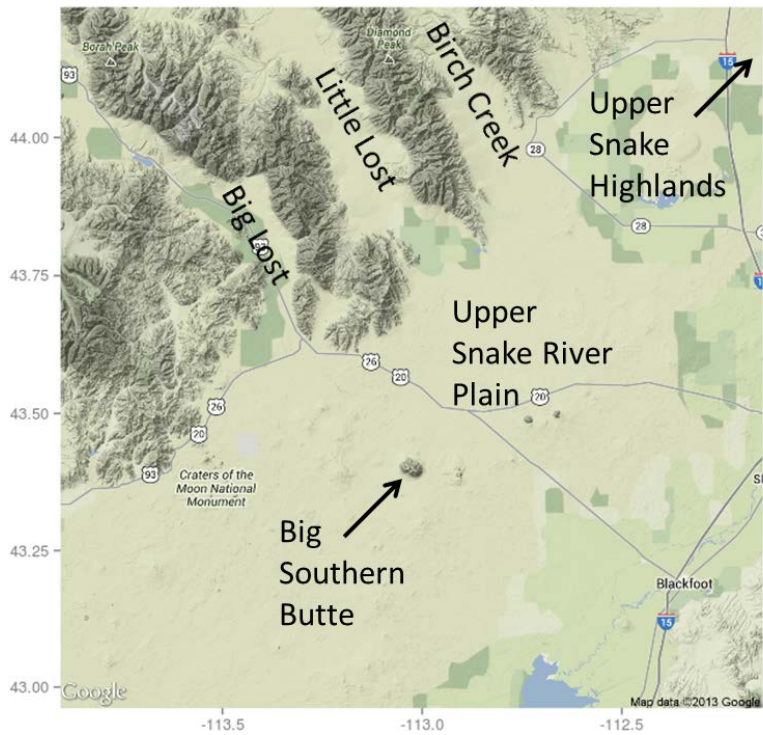


Figure 2. Snake River Plain and prominent drainages surrounding the Big Southern Butte study site.

High resolution observations of the near-surface wind field

B. W. Butler et al.

Title Page	
Abstract	Introduction
Conclusions	References
Tables	Figures
◀	▶
◀	▶
Back	Close
Full Screen / Esc	
Printer-friendly Version	
Interactive Discussion	



High resolution observations of the near-surface wind field

B. W. Butler et al.

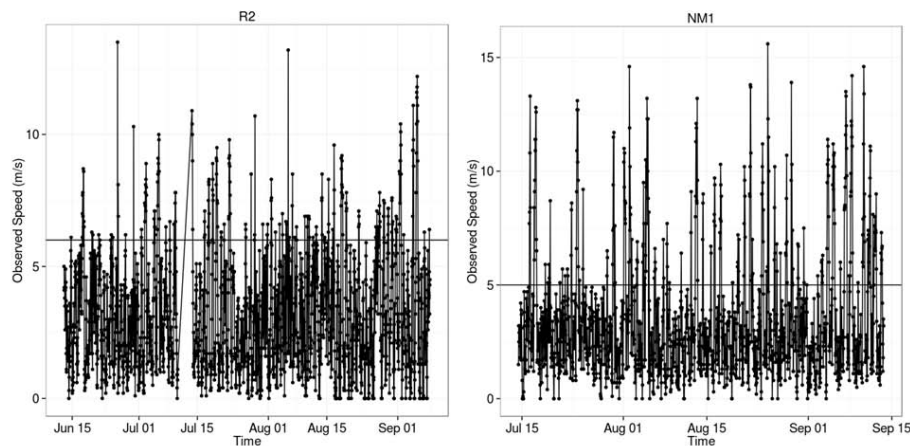


Figure 3. Observed hourly wind speeds for R2 at Big Southern Butte and NM1 at Salmon River Canyon. The horizontal line indicates the threshold speed chosen to partition synoptically driven events from diurnal events.

[Title Page](#)[Abstract](#)[Introduction](#)[Conclusions](#)[References](#)[Tables](#)[Figures](#)[Back](#)[Close](#)[Full Screen / Esc](#)[Printer-friendly Version](#)[Interactive Discussion](#)

High resolution observations of the near-surface wind field

B. W. Butler et al.

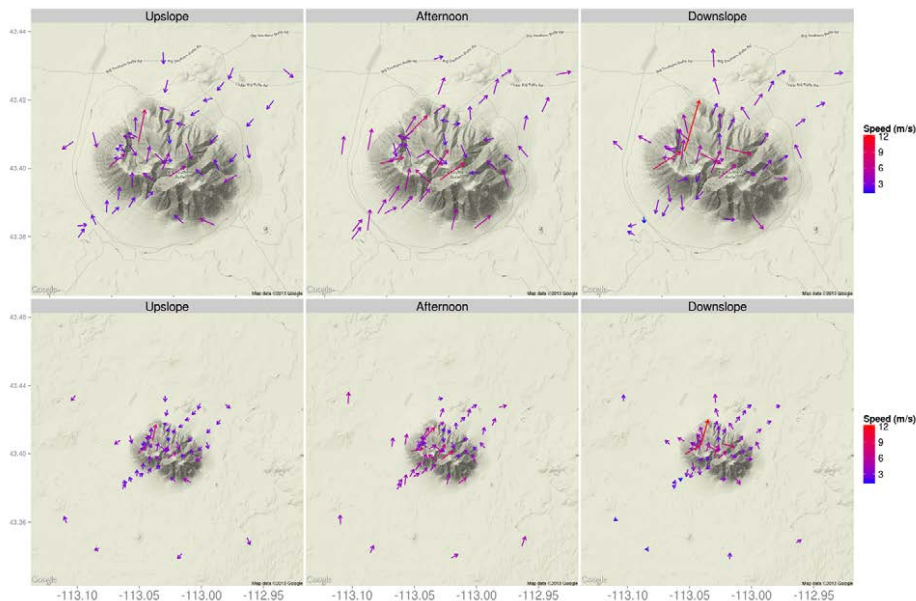


Figure 4. Upslope (11:00 LT), afternoon (16:00 LT), and downslope (00:00 LT) flow regimes at Big Southern Butte during periods of weak synoptic flow between June–September 2010. Vectors represent the average hourly flow at a given sensor. Vectors are centered on sensor locations. Periods of strong synoptic forcing were removed prior to averaging. Upper strip is zoomed in on the butte. Lower strip is zoomed out to show entire study area.

[Title Page](#)[Abstract](#)[Introduction](#)[Conclusions](#)[References](#)[Tables](#)[Figures](#)[◀](#)[▶](#)[◀](#)[▶](#)[Back](#)[Close](#)[Full Screen / Esc](#)[Printer-friendly Version](#)[Interactive Discussion](#)

High resolution observations of the near-surface wind field

B. W. Butler et al.

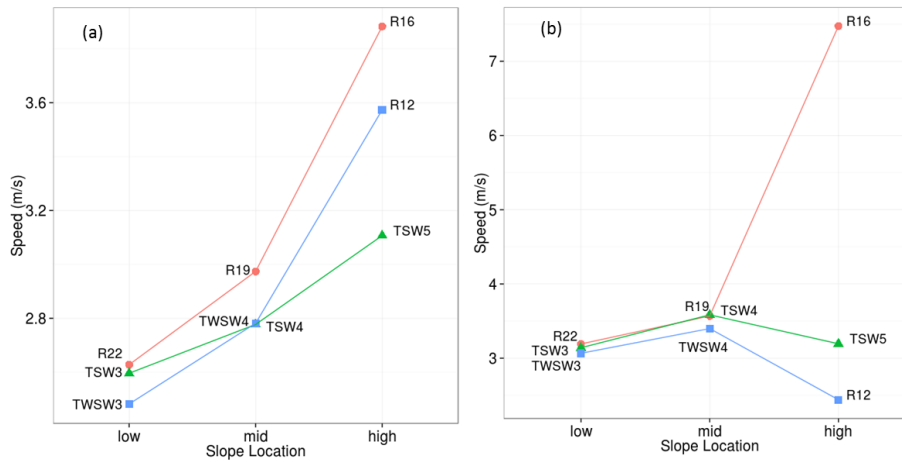


Figure 5. Average wind speeds for sensors at three slope locations (low, mid, and high) along three transects during the **(a)** upslope (11:00 LT) and **(b)** downslope (00:00 LT) flow regimes at Big Southern Butte.

High resolution observations of the near-surface wind field

B. W. Butler et al.

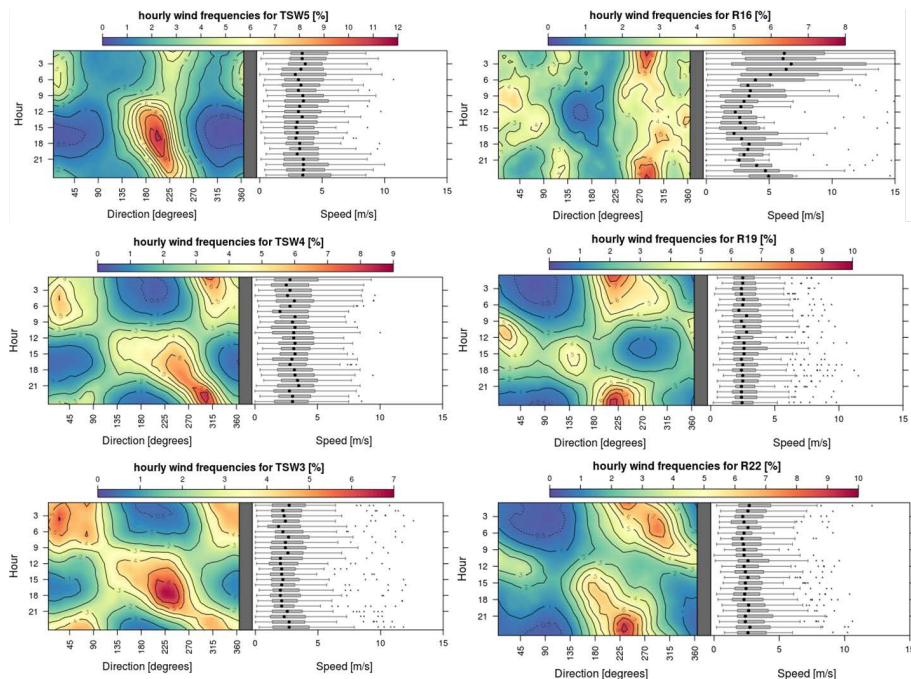


Figure 6. Contour plots of hourly wind frequencies and corresponding wind speeds for a transect on the southwest slope of Big Southern Butte (left panels) and a transect on the northeast slope of Big Southern Butte (right panels). Panels are ordered from higher elevation sensors (top panels) to lower elevation sensors (bottom panels). Periods of synoptic forcing were removed from this data.

Title Page

Abstract Introduction

Conclusions References

Tables Figures

◀ ▶

◀ ▶

Back Close

Full Screen / Esc

Printer-friendly Version

Interactive Discussion

High resolution observations of the near-surface wind field

B. W. Butler et al.

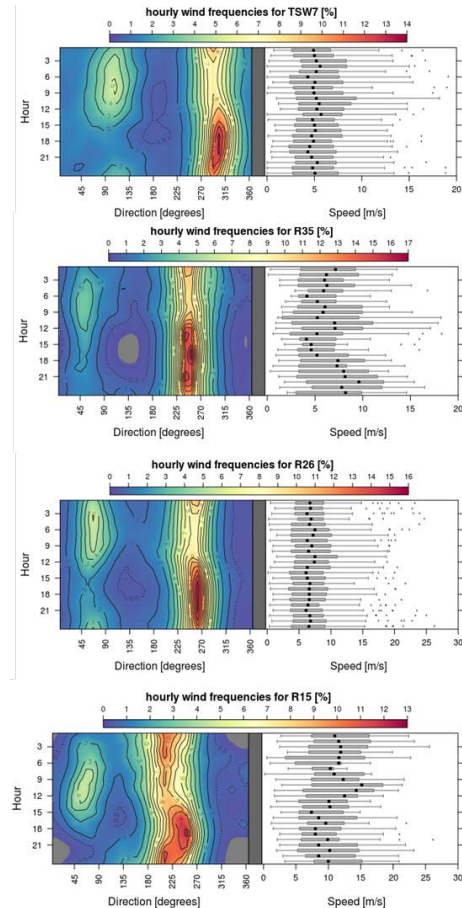


Figure 7. Contour plots of hourly wind frequencies and corresponding wind speeds for four ridgetop locations at Big Southern Butte. Periods of strong synoptic forcing were removed from this data.

[Title Page](#)[Abstract](#)[Introduction](#)[Conclusions](#)[References](#)[Tables](#)[Figures](#)[◀](#)[▶](#)[◀](#)[▶](#)[Back](#)[Close](#)[Full Screen / Esc](#)[Printer-friendly Version](#)[Interactive Discussion](#)

High resolution observations of the near-surface wind field

B. W. Butler et al.

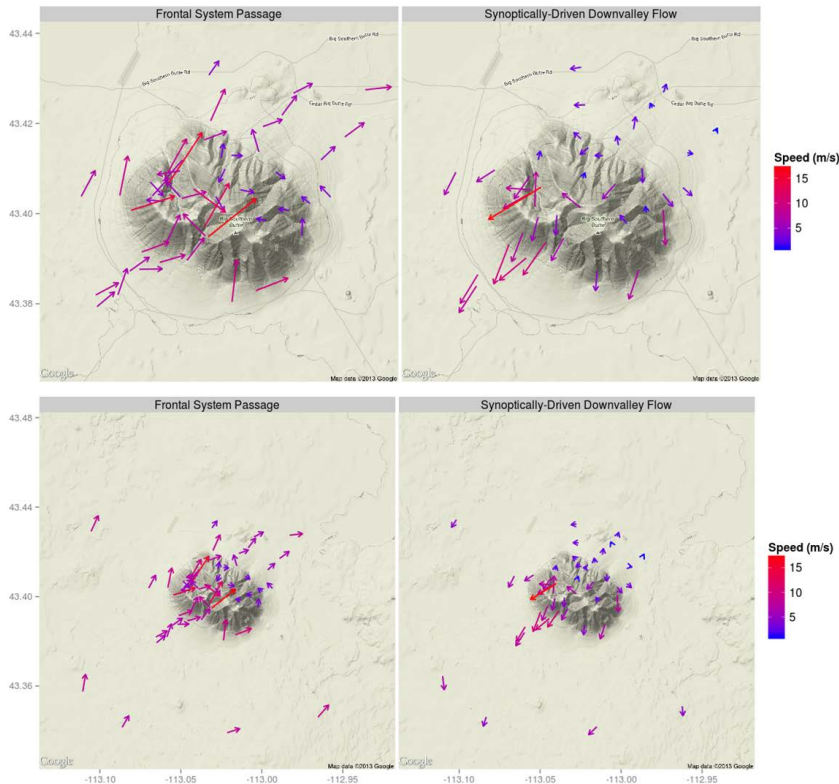


Figure 8. Characteristic synoptically-driven regime events during the passage of a frontal system (18:00 LT) and during synoptically-enhanced downvalley flow on the Snake River Plain (23:00 LT) at Big Southern Butte during June–September 2010. Vectors represent the average hourly flow at a given sensor. Periods of weak synoptic forcing were removed prior to averaging. Lower strip is zoomed out to show entire study area.

[Title Page](#)
[Abstract](#)
[Introduction](#)
[Conclusions](#)
[References](#)
[Tables](#)
[Figures](#)
[Back](#)
[Close](#)
[Full Screen / Esc](#)
[Printer-friendly Version](#)
[Interactive Discussion](#)

High resolution observations of the near-surface wind field

B. W. Butler et al.

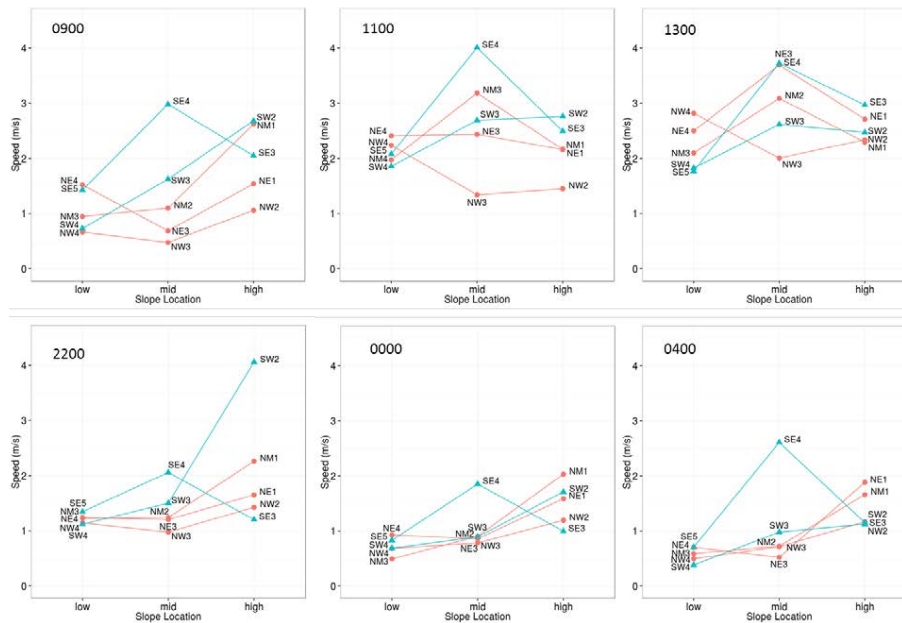


Figure 10. Average wind speeds for sensors at three slope locations (low, mid, and high) along five transects during three hours of the upslope (top panels) and downslope (bottom panels) flow regimes at Salmon River Canyon. Blue and red lines are transects on the south and north side of the river, respectively.

Title Page

Abstract

Introduction

Conclusions

References

Tables

Figures



Back

Close

Full Screen / Esc

Printer-friendly Version

Interactive Discussion



High resolution observations of the near-surface wind field

B. W. Butler et al.

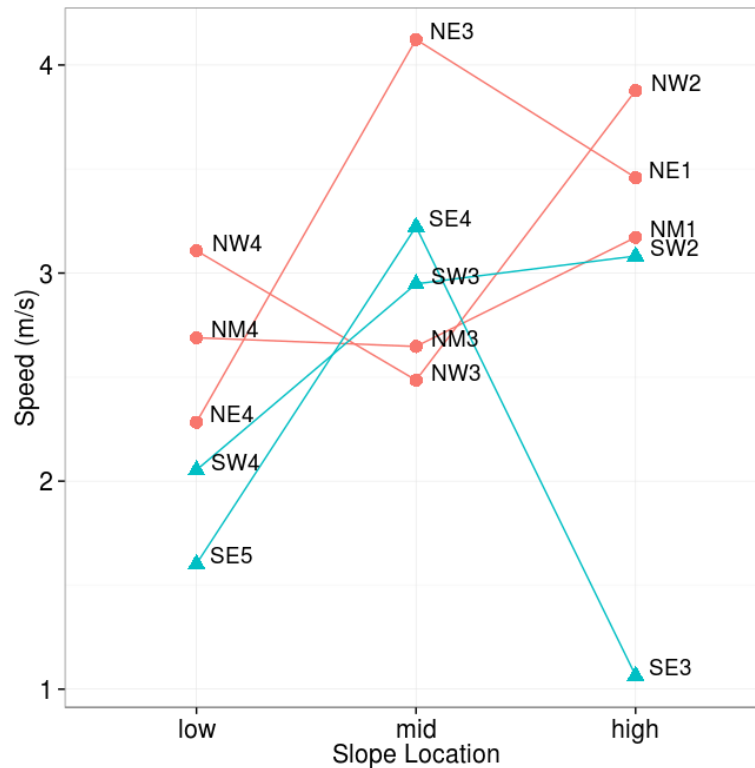


Figure 11. Average wind speeds for sensors at three slope locations (low, mid, and high) along five transects during the afternoon flow regime (17:00 LT) at Salmon River Canyon. Blue and red lines are transects on the south and north side of the river, respectively.

[Title Page](#)
[Abstract](#)
[Introduction](#)
[Conclusions](#)
[References](#)
[Tables](#)
[Figures](#)
[◀](#)
[▶](#)
[◀](#)
[▶](#)
[Back](#)
[Close](#)
[Full Screen / Esc](#)
[Printer-friendly Version](#)
[Interactive Discussion](#)


High resolution observations of the near-surface wind field

B. W. Butler et al.

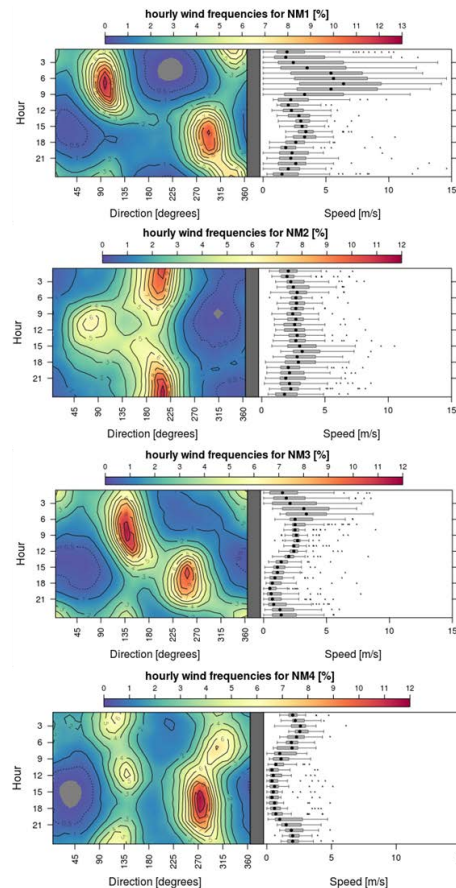


Figure 12. Contour plots of hourly wind frequencies and corresponding wind speeds for the NM transect at Salmon River Canyon. NM1 is near the ridgetop. NM4 is near the canyon bottom. All data were used.

[Title Page](#)[Abstract](#)[Introduction](#)[Conclusions](#)[References](#)[Tables](#)[Figures](#)[◀](#)[▶](#)[◀](#)[▶](#)[Back](#)[Close](#)[Full Screen / Esc](#)[Printer-friendly Version](#)[Interactive Discussion](#)

High resolution observations of the near-surface wind field

B. W. Butler et al.

Title Page

Abstract

Introduction

Conclusions

References

Tables

Figures



Back

Close

Full Screen / Esc

Printer-friendly Version

Interactive Discussion

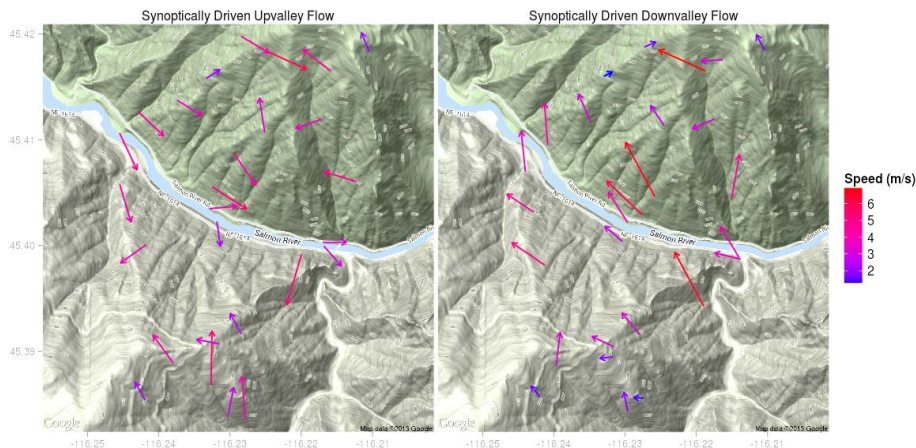


Figure 13. Characteristic synoptically driven upvalley flow (15:00 LT) and downvalley flow (11:00 LT) at Salmon River Canyon during July–September 2011. Vectors represent the average hourly flow at a given sensor. Periods of weak synoptic forcing were removed prior to averaging.

High resolution observations of the near-surface wind field

B. W. Butler et al.

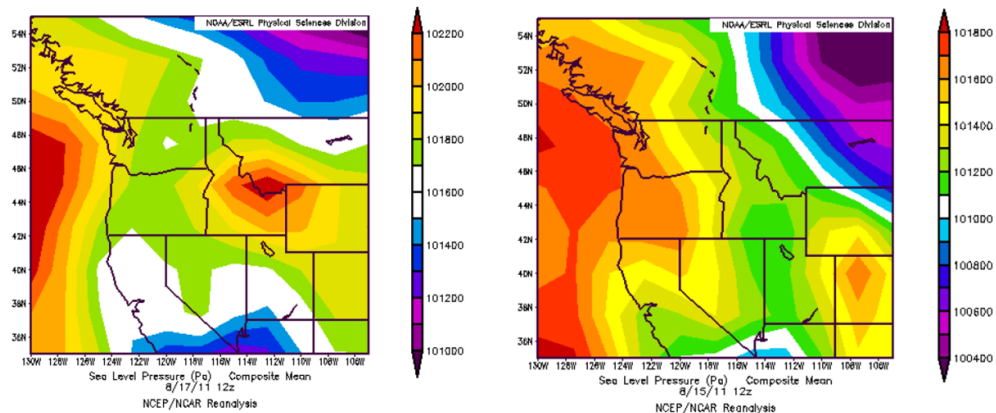


Figure 14. Synoptic-scale surface pressure conditions conducive to enhanced easterly flow (left) and typical diurnal flow scenarios (right) at Salmon River Canyon. (National Center for Environmental Prediction).

Title Page

Abstract

Introduction

Conclusions

References

Tables

Figures



Back

Close

Full Screen / Esc

Printer-friendly Version

Interactive Discussion



High resolution observations of the near-surface wind field

B. W. Butler et al.

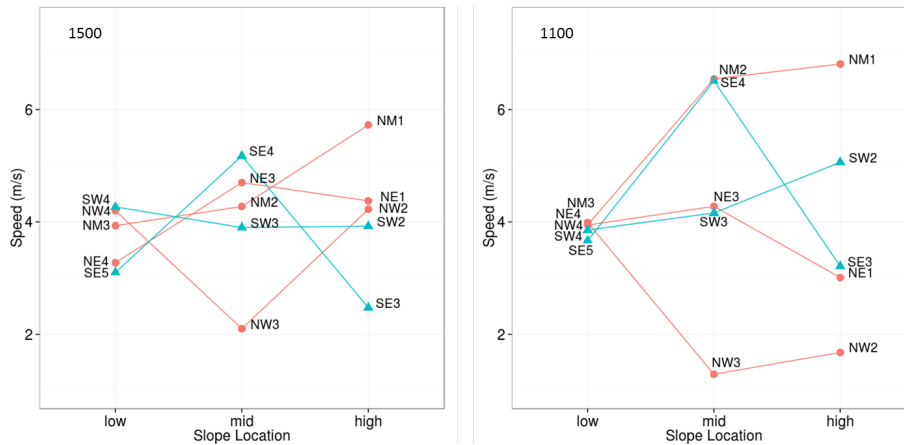


Figure 15. Average wind speeds for sensors at three slope locations (low, mid, and high) along five transects during the synoptically driven upvalley (left) and synoptically driven downvalley (right) flow regimes at Salmon River Canyon. Blue and red lines are transects on the south and north side of the river, respectively.

Title Page

Abstract

Introduction

Conclusions

References

Tables

Figures

◀

▶

◀

▶

Back

Close

Full Screen / Esc

Printer-friendly Version

Interactive Discussion

